

# Triaxial nuclear shapes from simple ratios of electric-quadrupole matrix elements

Elena Atanassova Lawrie<sup>a,b</sup>, José Nicolás Orce<sup>b,c</sup>

<sup>a</sup>*Themba LABS, National Research Foundation, PO Box 722, Somerset West 7129, South Africa*

<sup>b</sup>*National Institute for Theoretical and Computational Sciences (NITheCS), South Africa*

<sup>c</sup>*Department of Physics & Astronomy, University of the Western Cape, P/B X17, Bellville ZA-7535, South Africa*

---

## Abstract

Theoretical models often invoke triaxial nuclear shapes to explain elusive collective phenomena, but such assumptions are usually difficult to confirm experimentally. The only direct measurements of the nuclear axial asymmetry  $\gamma$  is based on rotational invariants of zero-coupled products of the electric-quadrupole (E2) operator, the Kumar-Cline sum rule analysis, which generally require knowledge of a large number of E2 matrix elements connecting the state of interest. We propose an alternative assumptions-free method to determine  $\gamma$  of even-even rotating nuclei using only two E2 matrix elements, which are among the easiest to measure. This approach is based on a simple description of nuclear rotation, where the underlying assumptions of the Davydov-Filippov model are either empirically proven or unnecessary. The  $\gamma$  values extracted here are found in agreement with the values deduced from Kumar-Cline sum rules measurements (where available), providing further evidence that the proposed approach represents a reliable, model-independent deduction of  $\gamma$ . The technique was applied to more than 60 deformed even-even rotating nuclei and the results indicate that rotating nuclei generally exhibit well-defined stable axially-asymmetric shapes.

*Keywords:* quadrupole deformation, triaxiality, electric-quadrupole matrix elements, multi-step Coulomb excitation, irrotational flow model, triaxial rotor model, model-independent evaluation of  $\gamma$

---

Triaxial shapes — like kiwis or flattened footballs — break the axial symmetry of a deformed object and are basic ingredients in theoretical models describing both the quantum world and the realm of general relativity, albeit its testing through direct experimental observations remains challenging. Triaxiality plays an important role in (i) nuclear fission [1], with its relevance to energy production; (ii) the radiative capture of neutrons in stellar explosions [2], responsible for the creation of heavy elements; (iii) the formation of some superdeformed bands in nuclei [3], and iv) the low-lying nuclear structure [4].

The majority of nuclei show quadrupole deformations [5, 6], described by two parameters,  $\beta_2$  and  $\gamma$ . Here,  $\beta_2$  defines the magnitude of the quadrupole deformation and  $\gamma$  the degree of axial asymmetry or triaxiality, where axially-symmetric deformations correspond to  $\gamma = 0^\circ$  (prolate) and  $\gamma = 60^\circ$  (oblate) while triaxial shapes to  $0^\circ < \gamma < 60^\circ$ . Global calculations of all even-even nuclei in the nuclear chart [7, 8] suggest that the

total energy of many nuclei decreases substantially if the nuclear shape has stable triaxial deformation.

Theoretical approaches where the  $\gamma$  degree of freedom plays a dominant role involve  $\gamma$  vibrations and rotations. The former may appear as (i) a dynamical feature of the nuclear shape, corresponding to small  $\gamma$  oscillations of the nuclear surface around an average axially symmetric shape [9], and (ii) as large-scale  $\gamma$  oscillations caused by the  $\gamma$ -softness of the nuclear shape, that may cover the whole range of  $\gamma$  between  $0^\circ$  and  $60^\circ$  [10]. In contrast, deformed nuclei with stable triaxial shape rotate around their three axes generating sets of rotational bands that can be described within the Davydov-Filippov (DF) model [11, 12, 13]. This rotation looks like the precession of a rotating top.

Triaxial deformation has often been inferred through indirect methods by comparing experimental observations with the predictions of theoretical models, based on (i) the splitting of the giant dipole resonance (GDR) into three dominant peaks [14, 15, 16, 17], (ii) the signature splitting and inversion in rotational bands [18, 19, 20, 21], (iii) the near-degeneracy of chiral partner bands [22, 23, 24], and (iv) the features of the tilted

---

*Email addresses:* ea.lawrie@ilabs.nrf.ac.za (Elena Atanassova Lawrie), jnorce@uwc.ac.za (José Nicolás Orce)  
*URL:* <https://nuclear.uwc.ac.za> (José Nicolás Orce)

precession and wobbling bands [25, 26]. Alternatively,  $\beta_2$  and  $\gamma$  can be extracted from potential energy surface calculations, e.g., total Routhian surface [27], Cranked Nilsson-Strutinsky [28], and beyond mean-field calculations of total energy surfaces and collective wave functions [29, 30, 4].

Rotational invariants represented as Kumar-Cline (KC) sums [31, 32] remain to date the only direct experimental technique to establish the magnitude of triaxiality,  $\gamma_{KC}$ , in the intrinsic frame of the nucleus. Such an analysis requires experimental data on a large number of electric-quadrupole (E2) matrix elements of up to sixth-order E2 invariants to evaluate also statistical fluctuations, which are hard to determine experimentally. Among more than 270 deformed rotating even-even nuclei with a ratio of excitation energies between the first  $4_1^+$  and  $2_1^+$  states of  $R_{4/2} \geq 2.4$  [33],  $\gamma_{KC}$  values have only been determined for 19; namely,  $^{74,76}\text{Ge}$  [34, 35],  $^{76}\text{Kr}$  [36],  $^{98}\text{Sr}$  [37],  $^{104}\text{Ru}$  [38],  $^{106-110}\text{Pd}$  [39, 40],  $^{148}\text{Nd}$  [41],  $^{166,168}\text{Er}$  [42, 43],  $^{172}\text{Yb}$  [44],  $^{182,184}\text{W}$  [45],  $^{186-192}\text{Os}$  [46] and  $^{194}\text{Pt}$  [46]. These are all stable nuclei, except for  $^{76}\text{Kr}$  [36] with a half-life of 14.8 h, and  $^{98}\text{Sr}$  [37] with a half-life of 0.653 s, where the corresponding E2 matrix elements were primarily extracted from multi-step Coulomb-excitation measurements [47]. The deduced  $\gamma_{KC}$  values indicate that all these nuclei present triaxial deformations, which highlights the need for establishing a simpler model-independent approach for evaluating triaxiality.

Recently, an assumption-free approach was proposed for even-even rotating nuclei through the generalized triaxial-rotor model (TR) with independent electric quadrupole and inertia tensors [48]. This approach is based on the DF model, but the moments of inertia (MoI) asymmetry is described through a new parameter  $\Gamma$ , in an independent way from the shape asymmetry  $\gamma$ . Thus the assumption of the DF model that the MoI follow the irrotational-flow dependence with respect to  $\gamma$  become redundant. The generalized TR model was then applied for the  $2_1^+$  and  $2_2^+$  states of 26 even-even rotating nuclei with  $R_{4/2} \geq 2.4$  [49, 50], for which experimental data on the required four E2 matrix elements were available. As it was applied to the  $2_1^+$  and  $2_2^+$  states only, it made the additional assumption of the DF model regarding the spin-dependence of the MoI also redundant; hence, providing an empirical, assumptions-free determination of the  $\gamma$  deformation for these nuclei. Moreover, all these nuclei were found to possess triaxial deformations, supporting the consideration that triaxiality might be a common feature for nuclei.

In this Letter, we propose to expand this approach and determine the magnitude of the nuclear triaxiality

of even-even rotating nuclei in the same assumption-free approach, but using only two E2 matrix elements. The number of required E2 matrix elements is reduced because we adopt the irrotational-flow dependence between the parameters  $\Gamma$  and  $\gamma$ . We consider that this dependence was proved within the assumptions-free generalized TR approach for 12 even-even nuclei [49] and for 13 more even-even rotating nuclei, discussed in this work. Thus, the proposed analysis for the  $2_1^+$  and  $2_2^+$  states, while remaining based on the DF equations allows us to determine the  $\gamma$  deformation of more than 60 even-even rotating nuclei in a simple, model-independent evaluation.

Deformed nuclei can easily be recognised by their large  $B(E2; 2_1^+ \rightarrow 0_1^+)$  reduced transition probabilities values (of  $\gtrsim 20$  Weisskopf units) connecting the first-excited  $2_1^+$  and the ground  $0_1^+$  states with an E2 transition. The  $B(E2)$  values for rotating nuclei are directly proportional to the square of the intrinsic quadrupole moment of the nucleus,  $Q_0$ , and the corresponding  $\langle I_1 K 2 0 | I_2 K \rangle$  Clebsch-Gordan coefficient [5, 51], and for axially-symmetric deformed nuclei,

$$B(E2; 0_1^+ \rightarrow 2_1^+) = \frac{5}{16\pi} Q_0^2, \quad (1)$$

where  $Q_0$  is related to  $\beta_2$  by [5]

$$Q_0 = \frac{3}{\sqrt{5}\pi} ZeR^2\beta_2 [1 + 0.16\beta_2], \quad (2)$$

with  $Z$  being the proton number,  $R = 1.2 A^{1/3}$  fm the radius of a nucleus with a sharp surface, and  $A = N + Z$  the atomic mass number with  $N$  the number of neutrons.

The Hamiltonian of a deformed rotating nucleus with stable triaxial deformation comprises simultaneous rotations around the nuclear axes,

$$\mathcal{H} = \frac{\hbar^2}{2\mathfrak{I}_1} \hat{I}_1^2 + \frac{\hbar^2}{2\mathfrak{I}_2} \hat{I}_2^2 + \frac{\hbar^2}{2\mathfrak{I}_3} \hat{I}_3^2, \quad (3)$$

where  $\hat{I}_k$  are the operators of the total angular momentum projections onto the body-fixed axes, and  $\mathfrak{I}_1$ ,  $\mathfrak{I}_2$ , and  $\mathfrak{I}_3$  the corresponding MoI. The DF model generally adopts two main assumptions about the nuclear rotation. Firstly, the relative ratios of  $\mathfrak{I}_1$ ,  $\mathfrak{I}_2$ , and  $\mathfrak{I}_3$  for a given  $\gamma$  deformation follow the irrotational-flow dependence,

$$\mathfrak{I}_k(\gamma) = \mathfrak{I}_0 \sin^2\left(\gamma - k\frac{2\pi}{3}\right), \quad (4)$$

with  $\mathfrak{I}_0$  the MoI of an axially symmetric nucleus with respect to an axis that is orthogonal to the axis of symmetry [52], and  $k = 1, 2, 3$ . In fact, the  $\gamma$  dependence in

Eq. 4 is more general than the irrotational-flow model (for details see Ref. [6], page 121). Secondly, the DF model needs an assumption about the spin dependence of the MoI. In the original DF model, the MoI remains constant as a function of spin, whereas in later applications variable moments of inertia [53] are often introduced.

Instead of adopting the  $\gamma$  dependence of Eq. 4, the generalized TR model describes the asymmetry in the three MoI independently from  $\gamma$ , by introducing a new MoI-asymmetry parameter  $\Gamma$  [48]. Accordingly, the E2 matrix elements connecting the  $0_1^+$ ,  $2_1^+$  and  $2_2^+$  states are given by

$$\langle 0_1^+ \parallel \hat{E}2 \parallel 2_1^+ \rangle = \sqrt{\frac{5}{16\pi}} Q_0 \cos(\gamma + \Gamma), \quad (5)$$

$$\begin{aligned} \langle 2_1^+ \parallel \hat{E}2 \parallel 2_1^+ \rangle &= -\sqrt{\frac{25}{56\pi}} Q_0 \cos(\gamma - 2\Gamma) \quad (6) \\ &= -\langle 2_2^+ \parallel \hat{E}2 \parallel 2_2^+ \rangle, \end{aligned}$$

$$\langle 2_1^+ \parallel \hat{E}2 \parallel 2_2^+ \rangle = \sqrt{\frac{25}{56\pi}} Q_0 \sin(\gamma - 2\Gamma), \quad (7)$$

$$\langle 0_1^+ \parallel \hat{E}2 \parallel 2_2^+ \rangle = \sqrt{\frac{5}{16\pi}} Q_0 \sin(\gamma + \Gamma). \quad (8)$$

Therefore, empirical values for the axial asymmetry of the shape of rotating nuclei ( $\gamma_{TR}$ ) and of the MoI ( $\Gamma_{TR}$ ) can be extracted from Eqs. 5, 6, 7, and 8 [49],

$$\gamma_{TR} = \frac{1}{3} \left[ 2 \tan^{-1} \left( \frac{\langle 0_1^+ \parallel \hat{E}2 \parallel 2_2^+ \rangle}{\langle 0_1^+ \parallel \hat{E}2 \parallel 2_1^+ \rangle} \right) + \tan^{-1} \left( -\frac{\langle 2_1^+ \parallel \hat{E}2 \parallel 2_2^+ \rangle}{\langle 2_1^+ \parallel \hat{E}2 \parallel 2_1^+ \rangle} \right) \right] \quad (9)$$

$$\Gamma_{TR} = \frac{1}{3} \left[ \tan^{-1} \left( \frac{\langle 0_1^+ \parallel \hat{E}2 \parallel 2_2^+ \rangle}{\langle 0_1^+ \parallel \hat{E}2 \parallel 2_1^+ \rangle} \right) - \tan^{-1} \left( -\frac{\langle 2_1^+ \parallel \hat{E}2 \parallel 2_2^+ \rangle}{\langle 2_1^+ \parallel \hat{E}2 \parallel 2_1^+ \rangle} \right) \right] \quad (10)$$

using four measured E2 matrix elements. Note that these equations remain assumptions-free for rotating nuclei because they are applied to the  $2^+$  states only; i.e., the spin-dependence of the MoI becomes irrelevant. Available experimental data allowed  $\gamma_{TR}$  and  $\Gamma_{TR}$  values to be deduced for 26 even-even rotating nuclei [49, 50], further testing whether  $\Gamma$  and  $\gamma$  are independent or may follow the irrotational-flow model dependence,

$$\Gamma(\gamma) = -\frac{1}{2} \cos^{-1} \left( \frac{\cos(4\gamma) + 2 \cos(2\gamma)}{\sqrt{9 - 8 \sin^2(3\gamma)}} \right). \quad (11)$$

Agreement validating Eq. 11 was reported for 12 even-even rotating nuclei with  $R_{4/2} > 2.7$  [49]. The same evaluation for all nuclei with  $R_{4/2} > 2.4$ , where experimental data on four E2 matrix elements are available is

shown in Fig. 1. Discrepancies are observed for  $^{76}\text{Kr}$  and  $^{194,196}\text{Pt}$ , probably arising from the mixed nature of the corresponding  $2_2^+$  states. Indeed, shape coexistence at low-excitation energy was confirmed in  $^{76}\text{Kr}$ , while the observed  $2_2^+$  states in the two Pt isotopes are observed to decay through transitions with E0 components [54], which also suggests the presence of co-existing shapes [55].

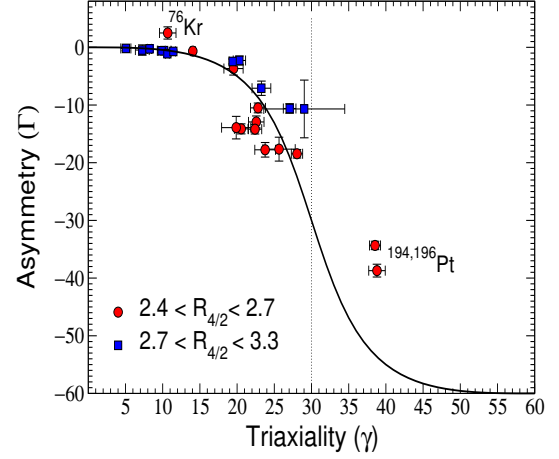


Figure 1: The irrotational-flow model  $\Gamma_{irr}(\gamma)$  (solid line) in comparison with empirical  $\gamma_{TR}$  and  $\Gamma_{TR}$  values for deformed even-even nuclei with  $R_{4/2}$  values between 2.4 and 3.3.

Henceforth, we extend the application of the generalized TR approach [49] by adopting Eq. 11 not as an assumption, but as an empirically established dependence. This allows the application of this model-independent approach to a much larger range of rotating nuclei.

Specifically, from Eqs. 5 and 6 we define the ratio  $R_{22/02}$  that is based on the two typically well-known  $\langle 2_1^+ \parallel \hat{E}2 \parallel 2_1^+ \rangle$  and  $\langle 0_1^+ \parallel \hat{E}2 \parallel 2_1^+ \rangle$  matrix elements,

$$R_{22/02} := \frac{\langle 2_1^+ \parallel \hat{E}2 \parallel 2_1^+ \rangle}{\langle 0_1^+ \parallel \hat{E}2 \parallel 2_1^+ \rangle} = -\sqrt{\frac{10}{7}} \frac{\cos(\gamma - 2\Gamma)}{\cos(\gamma + \Gamma)}, \quad (12)$$

which taking Eq. 11 into account becomes

$$R_{22/02}(\gamma) = -\sqrt{\frac{10}{7}} \frac{\cos \left( \gamma + \cos^{-1} \left( \frac{\cos(4\gamma) + 2 \cos(2\gamma)}{\sqrt{4 \cos(6\gamma) + 5}} \right) \right)}{\cos \left( \gamma - \frac{1}{2} \cos^{-1} \left( \frac{\cos(4\gamma) + 2 \cos(2\gamma)}{\sqrt{8 \cos^2(3\gamma) + 1}} \right) \right)}. \quad (13)$$

The function  $R_{22/02}(\gamma)$ , shown in the left panel of Fig. 2 (solid line), is continuous in the  $[0^\circ, 60^\circ]$   $\gamma$  range, varying smoothly between  $R_{22/02}(\gamma = 0^\circ) = -1.195$  (prolate) and  $R_{22/02}(\gamma = 60^\circ) = +1.195$  (oblate) and

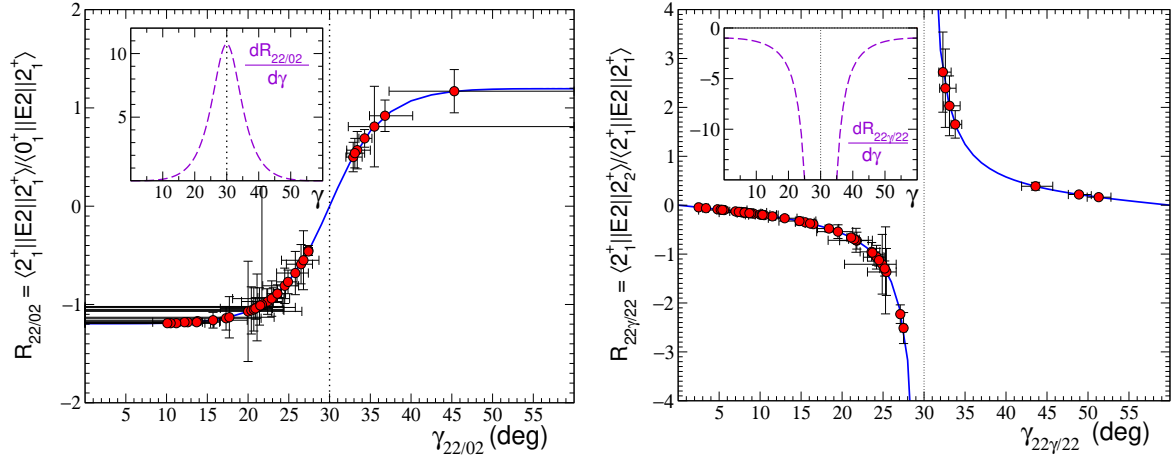


Figure 2:  $R_{22/02}$  (left) and  $R_{22\gamma/02}$  (right) ratios as a function of the  $\gamma$  deformation. The solid curves are calculated within the proposed here approach while the experimental data (circles) are calculated from available matrix elements for even-even nuclei with  $R_{4/2} > 2.4$ . The corresponding  $\gamma$  values are extracted from the theoretical (solid line) curves. The first derivatives (dashed lines) reveal high sensitivity to the  $\gamma$  degree of freedom.

vanishing for  $\gamma = 30^\circ$ . Therefore, one can deduce the  $\gamma_{R22/02}$  deformation of an even-even rotating nucleus using the  $R_{22/02}$  curve together with  $R_{22/02}$  determined from the experimentally-determined matrix elements. The first derivative  $\frac{dR_{22/02}}{d\gamma}$  (dashed line) shown in the inset of Fig. 2 is also continuous, with a maximum at  $\gamma = 30^\circ$ . This method allows the precise determination of  $\gamma$  values for nuclei with large asymmetry, while considerable uncertainties are expected for nuclei with nearly axially-symmetric shapes.

Following this approach, we have evaluated  $R_{22/02}$  and  $\gamma_{R22/02}$  for 63 deformed even-even nuclei with  $R_{4/2} > 2.4$ . These values are shown in the left panel of Fig. 2 and listed in Table 1 along with the corresponding  $\langle 2_1^+ || \hat{E}2 || 2_1^+ \rangle$  and  $\langle 0_1^+ || \hat{E}2 || 2_1^+ \rangle$  matrix elements, which were deduced from the corresponding evaluations of  $Q_s(2_1^+)$  [56] and  $B(E2; 0_1^+ \rightarrow 2_1^+)$  [57] values, respectively, unless more recent and precise experimental data were available. Deformations are labelled as prolate or oblate in the few cases where  $|R_{22/02}| > 1.195$ , depending on the sign of  $R_{22/02}$ . There was no sign measured for the  $\langle 2_1^+ || \hat{E}2 || 2_1^+ \rangle$  matrix element of  $^{160}\text{Dy}$ , we adopted negative sign in agreement with the systematics, see note p in Table 1. The sign of the  $\langle 2_1^+ || \hat{E}2 || 2_1^+ \rangle$  matrix element in  $^{76}\text{Kr}$  was changed to positive (together with the same change for the  $\langle 2_1^+ || \hat{E}2 || 0_1^+ \rangle$  matrix element, which keeps the sign of the  $P_3$  term unchanged [58]), in order to comply with the systematically observed prolate-type shapes of the neighbouring nuclei. The  $P_3$  term is defined in Coulomb-excitation theory [59] as the interference between the direct excitation ampli-

tude  $0_1^+ \rightarrow 2_1^+$  and the indirect one,  $0_1^+ \rightarrow 2_1^+ \rightarrow 2_1^+$ , and depends on the product of the three related matrix elements; Refs. [36, 60]). One of the nice achievements of the generalized TR model is that it can explain the sign of the  $P_3$  term [58].

For some of the nuclei analysed in our work there are previous assumptions-free evaluations of  $\gamma_{TR}$  and/or  $\gamma_{KC}$ . A comparison of these values with those established in the proposed approach shows an overall agreement, with most values overlapping at the one- or two- $\sigma$  level, see the top panels of Fig. 3. Deviations are noticeable for the  $^{194,196}\text{Pt}$  nuclei where, as mentioned above, shape-coexisting effects are expected to play a role in the formation of the  $2_1^+$  states.

Thus, the  $\gamma$  deformations were evaluated in an assumptions-free method for thirty even-even rotating nuclei beyond those for which  $\gamma_{TR}$  and  $\gamma_{KC}$  were available. Many of these nuclei were found consistent with small triaxial deformations, not excluding axial symmetry, but we also identified a considerable number of triaxial nuclei, including  $^{56}\text{Fe}$  ( $\gamma_{R22/02} = 22.4^{+1.8}_{-3.2}$ ),  $^{78}\text{Kr}$  ( $\gamma_{R22/02} = 21.7^{+1.0}_{-1.3}$ ),  $^{152}\text{Sm}$  ( $\gamma_{R22/02} = 12.6^{+1.8}_{-4.3}$ ),  $^{170}\text{Er}$  ( $\gamma_{R22/02} = 20.9^{+2.1}_{-4.4}$ ),  $^{192}\text{Pt}$  ( $\gamma_{R22/02} = 33.4^{+1.6}_{-1.3}$ ),  $^{198}\text{Pt}$  ( $\gamma_{R22/02} = 33.2^{+1.2}_{-1.0}$ ), and  $^{198}\text{Hg}$  ( $\gamma_{R22/02} = 36.8^{+3.4}_{-1.9}$ ). It should also be noted that  $\gamma$  values inferred from this analysis are fully independent of the presence and features of the  $2_1^+$   $\gamma$  band. For instance, it allows the assignment of triaxiality for nuclei where the  $\gamma$  band has not yet been established, as we did for  $^{56}\text{Fe}$ . In addition, it permits an evaluation of triaxiality for nuclei where the  $2_1^+$  band is competing with other shape-coexisting structures and

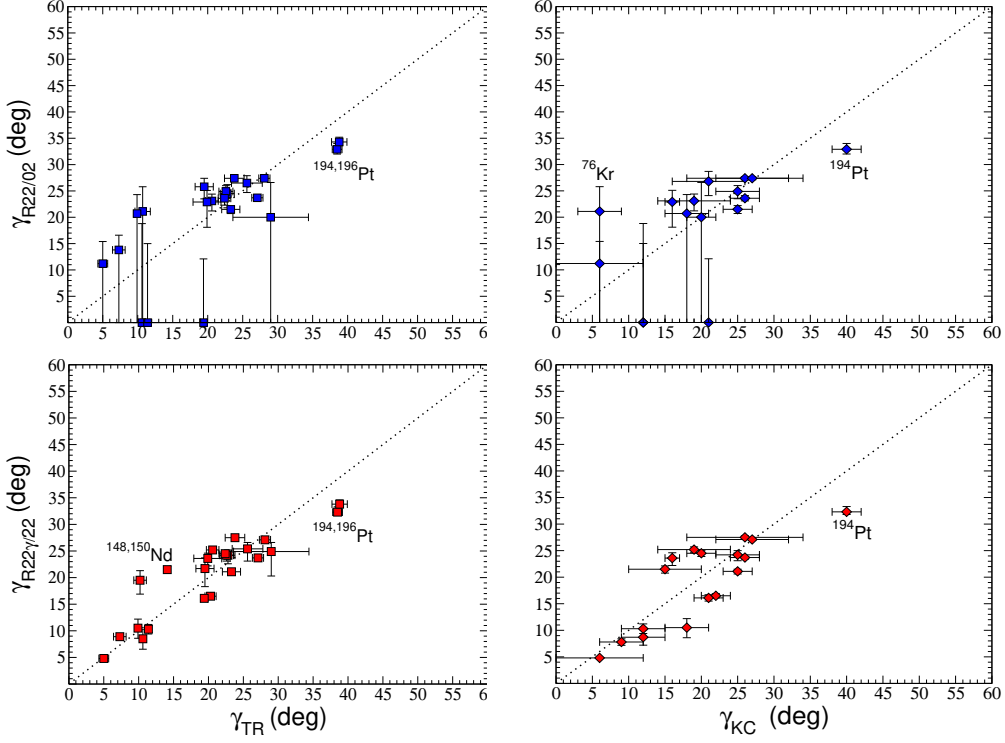


Figure 3: Triaxial deformations  $\gamma_{R_{22/02}}$  (top panels) and  $\gamma_{R_{22/22}}$  (bottom panels) versus  $\gamma_{TR}$  (left) and  $\gamma_{KC}$  (right).

is, therefore, mixed. For instance, we have inferred triaxiality for  $^{78}\text{Kr}$ ,  $^{152}\text{Sm}$ , and  $^{170}\text{Er}$ , where strong shape-coexisting phenomena occur [61, 62, 63, 55], based entirely on the matrix elements of their  $2_1^+$  states. We have also established triaxial deformations for the  $^{192,198}\text{Pt}$  isotopes that are in agreement with the systematics (similar to the available  $\gamma_{KC}$  value of the neighbouring  $^{196}\text{Pt}$  isotope [46, 64]) and proposed a triaxial shape for  $^{198}\text{Hg}$ , in contrast to the common assumption that the heavy Hg isotopes have axially-symmetric oblate deformations. More details about the structural implications of these results will be presented in a separate manuscript.

We have also defined another ratio of matrix elements,  $R_{22\gamma/22}$ ,

$$R_{22\gamma/22} := \frac{\langle 2_1^+ \parallel \hat{E}2 \parallel 2_\gamma^+ \rangle}{\langle 2_1^+ \parallel \hat{E}2 \parallel 2_1^+ \rangle} = -\tan(\gamma - 2\Gamma), \quad (14)$$

which allows to deduce nuclear triaxiality. Again, using

Eq. 11,

$$R_{22\gamma/22}(\gamma) = -\tan\left(\gamma + \cos^{-1}\left(\frac{\cos(4\gamma) + 2\cos(2\gamma)}{\sqrt{9 - 8\sin^2(3\gamma)}}\right)\right). \quad (15)$$

The function  $R_{22\gamma/22}(\gamma)$  is shown in the right panel of Fig. 2 (solid line), while its first derivative is plotted in the inset (dashed line). This ratio has an advantage over  $R_{22/02}$  because of its sensitivity to  $\gamma$  throughout the full  $[0^\circ, 60^\circ]$  range. It can be applied to all even-even rotating nuclei where the  $2_\gamma^+$  band head is well established, and not affected by shape co-existence or other phenomena. We have thus examined the available data for  $\langle 2_1^+ \parallel \hat{E}2 \parallel 2_\gamma^+ \rangle$  matrix elements in all deformed even-even rotating nuclei with  $R_{4/2} > 2.4$ , as listed in Table 1. In most cases the matrix element is deduced from the measured  $B(E2; 2_\gamma^+ \rightarrow 2_1^+)$  value.

In order to test this approach we have first calculated the  $R_{22\gamma/22}$  ratios and the corresponding  $\gamma_{R_{22\gamma/22}}$  values for the deformed even-even nuclei where  $\gamma_{TR}$  and/or  $\gamma_{KC}$  are available. Comparisons of  $\gamma_{R_{22\gamma/22}}$  vs  $\gamma_{TR}$  and  $\gamma_{R_{22\gamma/22}}$  vs  $\gamma_{KC}$  are shown in the bottom left and right panels of Fig. 3, respectively. Except for  $^{148,150}\text{Nd}$  and  $^{194,196}\text{Pt}$ , there

Table 1: The transitional and diagonal matrix elements (in units of eb) used to calculate the  $R_{22/02}$  and  $R_{22\gamma/02}$  ratios and the extracted  $\gamma$  deformation based on these ratios. For comparison the  $\gamma$  deformations deduced wherever possible using four matrix elements and using the Kumar-Cline rule are also listed. The data for the diagonal  $\langle 2_1^+ \parallel \hat{E}2 \parallel 2_1^+ \rangle$  as well as the transitional  $\langle 0_1^+ \parallel \hat{E}2 \parallel 2_1^+ \rangle$  and  $\langle 2_1^+ \parallel \hat{E}2 \parallel 2_1^+ \rangle$  matrix elements are taken from Refs. [56, 57, 33], unless stated differently.

Nucleus	$\langle 2_1^+ \parallel \hat{E}2 \parallel 2_1^+ \rangle$	$\langle 0_1^+ \parallel \hat{E}2 \parallel 2_1^+ \rangle$	$\langle 2_1^+ \parallel \hat{E}2 \parallel 2_1^+ \rangle$	$\gamma_{R22/02}$	$\gamma_{R22\gamma/02}$	$\gamma_{TR}$	$\gamma_{KC}$
<sup>12</sup> C	0.125(24) <sup>a</sup>	0.063(2)		oblate			
<sup>20</sup> Ne	-0.303(40)	0.182(4)	0.052(3)	prolate	9.2 <sup>+1.1</sup> <sub>-1.2</sub>		
<sup>22</sup> Ne	-0.284(16) <sup>b</sup>	0.152(1)	0.043(17)	prolate	8.1 <sup>+2.7</sup> <sub>-3.1</sub>		
<sup>22</sup> Mg	-0.57(57) <sup>b</sup>	0.184(43)		0 <sup>+30.5</sup> <sub>-0</sub>			
<sup>24</sup> Mg	-0.237(26) <sup>c</sup>	0.209(2)	0.083(3)	17.3 <sup>+4.3</sup> <sub>-17.3</sub>	15.5 <sup>+1.1</sup> <sub>-1.2</sub>		
<sup>28</sup> Si	0.211(40)	0.181(2)		45.3 <sup>+14.7</sup> <sub>-8.0</sub>			
<sup>50</sup> Cr	-0.475(92)	0.324(5)		0 <sup>+13.1</sup> <sub>-0</sub>			
<sup>56</sup> Fe	-0.303(40)	0.313(3)	0.145(9)	22.4 <sup>+1.8</sup> <sub>-3.2</sub>	18.4 <sup>+1.2</sup> <sub>-1.4</sub>		
<sup>58</sup> Fe	-0.356(66)	0.349(9)	0.258(39)	21.4 <sup>+3.0</sup> <sub>-21.4</sub>	21.8 <sup>+1.4</sup> <sub>-2.1</sub>		
<sup>62</sup> Fe	-0.11(53) <sup>d</sup>	0.319(97)		28.2 <sup>+31.8</sup> <sub>-28.2</sub>			
<sup>74</sup> Ge	-0.251(26)	0.553(14)	0.630(44)	27.4 <sup>+0.3</sup> <sub>-0.3</sub>	27.5 <sup>+0.3</sup> <sub>-0.4</sub>	23.8(14)	26(8)
<sup>76</sup> Ge	-0.240(20) <sup>e</sup>	0.526(20) <sup>e</sup>	0.535(7) <sup>e</sup>	27.3 <sup>+0.3</sup> <sub>-0.3</sub>	27.1 <sup>+0.2</sup> <sub>-0.2</sub>	28.1(8)	27(5)
<sup>80</sup> Ge	-0.61(41) <sup>f</sup>	0.408(10) <sup>f</sup>	<  0.8  <sup>f</sup>	0 <sup>+27.2</sup> <sub>-0</sub>	<25.3 or >34.7		
<sup>78</sup> Se	-0.34(12)	0.586(10)	0.469(19)	26.5 <sup>+1.4</sup> <sub>-1.8</sub>	25.4 <sup>+1.2</sup> <sub>-2.3</sub>	25.6(22)	
<sup>80</sup> Se	-0.409(92)	0.502(8)	0.435(12)	24.5 <sup>+1.7</sup> <sub>-2.7</sub>	24.2 <sup>+1.0</sup> <sub>-1.6</sub>	22.8(10)	
<sup>82</sup> Se	-0.290(92)	0.428(12)	0.208(25)	25.8 <sup>+1.6</sup> <sub>-2.3</sub>	21.7 <sup>+2.0</sup> <sub>-3.4</sub>	19.5(13)	
<sup>76</sup> Kr	-0.9(3) <sup>g</sup>	0.871(15)	0.09(4) <sup>g,o</sup>	21.1 <sup>+4.7</sup> <sub>-21.1</sub>	5.6 <sup>+2.8</sup> <sub>-3.1</sub>	10.7(1.1)	6(3)
<sup>78</sup> Kr	-0.80(4) <sup>h</sup>	0.796(10)	0.26(6) <sup>h</sup>	21.7 <sup>+1.0</sup> <sub>-1.2</sub>	14.8 <sup>+2.0</sup> <sub>-2.5</sub>		
<sup>98</sup> Sr	-0.63(32) <sup>i</sup>	1.14(20)		26.8 <sup>+1.9</sup> <sub>-2.7</sub>			21(3)
<sup>104</sup> Ru	-0.71(11) <sup>j</sup>	0.917(25) <sup>j</sup>	0.75(4) <sup>j</sup>	24.9 <sup>+1.1</sup> <sub>-1.4</sub>	24.2 <sup>+0.8</sup> <sub>-1.1</sub>	22.6(10)	25(3)
<sup>110</sup> Ru	-1.10(52) <sup>k</sup>	1.022(37) <sup>k</sup>	1.32(25) <sup>k</sup>	20.0 <sup>+6.6</sup> <sub>-20.0</sub>	24.9 <sup>+1.7</sup> <sub>-4.6</sub>	29.0(54)	
<sup>106</sup> Pd	-0.72(7) <sup>l</sup>	0.812(10)	0.810(37) <sup>s</sup>	23.6 <sup>+1.0</sup> <sub>-1.3</sub>	24.5 <sup>+0.5</sup> <sub>-0.6</sub>	22.4(9)	20(2)
<sup>108</sup> Pd	-0.810(90) <sup>l</sup>	0.874(11)	1.049(44)	23.1 <sup>+1.3</sup> <sub>-1.9</sub>	25.2 <sup>+0.5</sup> <sub>-0.6</sub>	20.6(9)	19(5)
<sup>110</sup> Pd	-0.87(17) <sup>m</sup>	0.930(12)	0.830(28)	22.9 <sup>+2.2</sup> <sub>-4.8</sub>	23.6 <sup>+1.0</sup> <sub>-1.4</sub>	19.9(20)	16(1)
<sup>130</sup> Ba	-1.35(20)	1.067(22)		0 <sup>+19.9</sup> <sub>-0</sub>			
<sup>148</sup> Nd	-1.93(18)	1.157(13)	1.342(17)	prolate	21.5 <sup>+0.6</sup> <sub>-0.7</sub>	14.1(3)	15(5)
<sup>150</sup> Nd	-2.64(66)	1.645(9)	1.427(9)	prolate	19.5 <sup>+1.8</sup> <sub>-2.6</sub>	10.2(9)	
<sup>152</sup> Sm	-2.198(21)	1.860(1)	0.422(29)	12.6 <sup>+1.8</sup> <sub>-4.3</sub>	10 <sup>+0.6</sup> <sub>-0.6</sub>		
<sup>154</sup> Sm	-2.467(53)	2.084(11)	0.108(8)	12.2 <sup>+3.6</sup> <sub>-12.2</sub>	2.5 <sup>+0.2</sup> <sub>-0.2</sub>		
<sup>154</sup> Gd	-2.401(53)	1.968(4)	0.549(22) <sup>s</sup>	0 <sup>+7.9</sup> <sub>-0</sub>	11.5 <sup>+0.4</sup> <sub>-0.4</sub>		
<sup>156</sup> Gd	-2.546(53)	2.168(25)	0.425(7)	13.8 <sup>+2.8</sup> <sub>-13.8</sub>	8.9 <sup>+0.2</sup> <sub>-0.2</sub>	7.3(9)	
<sup>158</sup> Gd	-2.652(53)	2.256(24)	0.390(23)	13.7 <sup>+2.8</sup> <sub>-13.7</sub>	7.9 <sup>+0.4</sup> <sub>-0.4</sub>		
<sup>160</sup> Gd	-2.744(53)	2.277(3)	0.166(16)	0 <sup>+12.5</sup> <sub>-0</sub>	3.43 <sup>+0.3</sup> <sub>-0.4</sub>		
<sup>160</sup> Dy	-2.38(53) <sup>p</sup>	2.247(9)	0.468(17)	20.4 <sup>+4.0</sup> <sub>-20.4</sub>	10.2 <sup>+1.8</sup> <sub>-2.0</sub>		
<sup>164</sup> Dy	-2.74(20)	2.370(14)	0.444(18)	15.7 <sup>+4.2</sup> <sub>-15.7</sub>	8.6 <sup>+0.6</sup> <sub>-0.6</sub>		
<sup>166</sup> Er	-2.51(53)	2.397(19)	0.510(16)	20.7 <sup>+3.6</sup> <sub>-20.7</sub>	10.5 <sup>+1.7</sup> <sub>-1.9</sub>	9.9(5)	18(3)
<sup>168</sup> Er	-3.25(25) <sup>n</sup>	2.43(7) <sup>n</sup>	0.47(2) <sup>n</sup>	prolate	7.8 <sup>+0.6</sup> <sub>-0.6</sub>	8.2(3)	9(3)
<sup>170</sup> Er	-2.51(27)	2.416(14)	> 0.385	20.9 <sup>+2.1</sup> <sub>-4.3</sub>	> 8.3		
<sup>170</sup> Yb	-2.876(40)	2.392(15)	0.366(38) <sup>r</sup>	0 <sup>+12</sup> <sub>-0</sub>	7.0 <sup>+0.7</sup> <sub>-0.7</sub>		
<sup>172</sup> Yb	-2.929(53)	2.468(30)	0.250(6)	11.2 <sup>+4.2</sup> <sub>-11.2</sub>	4.8 <sup>+0.1</sup> <sub>-0.1</sub>	5.0(7)	6(6)
<sup>174</sup> Yb	-2.876(66)	2.419(33)	0.269(27) <sup>r</sup>	10.5 <sup>+5.3</sup> <sub>-10.5</sub>	5.2 <sup>+0.5</sup> <sub>-0.5</sub>		
<sup>176</sup> Yb	-3.008(79)	2.278(20)	0.289(19)	prolate	5.4 <sup>+0.4</sup> <sub>-0.4</sub>		
<sup>176</sup> Hf	-2.771(26)	2.328(37)	0.387(36) <sup>r</sup>	10.1 <sup>+4.6</sup> <sub>-10.1</sub>	7.6 <sup>+0.6</sup> <sub>-0.6</sub>		
<sup>178</sup> Hf	-2.665(26)	2.176(145)	0.362(12)	0 <sup>+16.9</sup> <sub>-0</sub>	7.4 <sup>+0.2</sup> <sub>-0.2</sub>		

Nucleus	$\langle 2_1^+ \parallel \hat{E}2 \parallel 2_1^+ \rangle$	$\langle 0_1^+ \parallel \hat{E}2 \parallel 2_1^+ \rangle$	$\langle 2_1^+ \parallel \hat{E}2 \parallel 2_2^+ \rangle$	$\gamma_{R22/02}$	$\gamma_{R22\gamma/22}$	$\gamma_{TR}$	$\gamma_{KC}$
<sup>180</sup> Hf	-2.639(26)	2.156(1)	0.396(23)	prolate	8.1 <sup>+0.4</sup> <sub>-0.4</sub>		
<sup>180</sup> W	-2.77(53)	2.037(34)		0 <sup>+19</sup> <sub>-0</sub>			
<sup>182</sup> W	-2.77(53)	2.031(10)	0.454(6) <sup>s</sup>	0 <sup>+18.8</sup> <sub>-0</sub>	8.7 <sup>+1.4</sup> <sub>-1.5</sub>	10.6(2)	12(3)
<sup>184</sup> W	-2.51(27)	1.925(9)	0.497(7)	0 <sup>+15</sup> <sub>-0</sub>	10.3 <sup>+0.9</sup> <sub>-0.9</sub>	11.4(3)	12(3)
<sup>186</sup> W	-2.11(40)	1.871(10)	0.564(20)	17.7 <sup>+5.5</sup> <sub>-17.7</sub>	13.0 <sup>+1.5</sup> <sub>-2.0</sub>		
<sup>184</sup> Os	-3.6(16)	1.793(22)		0 <sup>+18.9</sup> <sub>-0</sub>			
<sup>186</sup> Os	-2.151(53)	1.750(21)	0.835(32)	prolate	16.5 <sup>+0.4</sup> <sub>-0.4</sub>	20.3(8)	22(2)
<sup>188</sup> Os	-1.926(53)	1.581(11)	0.720(40)	0 <sup>+12.1</sup> <sub>-0</sub>	16.1 <sup>+0.6</sup> <sub>-0.6</sub>	19.4(5)	21(2)
<sup>190</sup> Os	-1.557(40)	1.534(29)	1.028(54)	21.5 <sup>+0.7</sup> <sub>-0.8</sub>	21.1 <sup>+0.4</sup> <sub>-0.5</sub>	23.3(13)	25(2)
<sup>192</sup> Os	-1.267(40)	1.425(35)	1.230(35)	23.6 <sup>+0.5</sup> <sub>-0.5</sub>	23.7 <sup>+0.2</sup> <sub>-0.3</sub>	27.1(8)	26(2)
<sup>192</sup> Pt	0.79(27)	1.393(23)	1.894(61)	33.4 <sup>+1.6</sup> <sub>-1.3</sub>	32.6 <sup>+1.3</sup> <sub>-0.7</sub>		
<sup>194</sup> Pt	0.63(0.19)	1.277(27)	1.72(12) <sup>s</sup>	32.9 <sup>+1.1</sup> <sub>-0.9</sub>	32.3 <sup>+1.0</sup> <sub>-0.5</sub>	38.5(7)	40(2)
<sup>196</sup> Pt	0.82(0.11)	1.184(29)	1.35(15) <sup>s</sup>	34.3 <sup>+0.9</sup> <sub>-0.7</sub>	33.8 <sup>+0.8</sup> <sub>-0.5</sub>	38.8(11)	
<sup>198</sup> Pt	0.55(16)	1.035(24)	1.13(0.11)	33.1 <sup>+1.2</sup> <sub>-1.0</sub>	33.1 <sup>+1.3</sup> <sub>-0.7</sub>		
<sup>198</sup> Hg	0.90(0.16)	0.980(4)	0.147(9)	36.8 <sup>+3.4</sup> <sub>-1.9</sub>	51.3 <sup>+1.5</sup> <sub>-1.4</sub>		
<sup>200</sup> Hg	1.27(0.15)	0.925(15)	0.276(31)	oblate	48.9 <sup>+1.5</sup> <sub>-1.3</sub>		
<sup>202</sup> Hg	1.15(0.18)	0.784(13)	0.444(59)	oblate	43.6 <sup>+2.1</sup> <sub>-1.7</sub>		
<sup>204</sup> Hg	0.53(27)	0.651(16)		35.5 <sup>+24.5</sup> <sub>-3.2</sub>			

<sup>a</sup> from Ref. [65]; <sup>b</sup> from Ref. [66]; <sup>c</sup> from Ref. [67]; <sup>d</sup> from Ref. [68]; <sup>e</sup> from Ref. [35]; <sup>f</sup> from Ref. [60]; <sup>g</sup> from Ref. [36]; <sup>h</sup> from Ref. [61]; <sup>i</sup> from Ref. [37]; <sup>j</sup> from Ref. [38]; <sup>k</sup> from Ref. [69]; <sup>l</sup> from Ref. [39]; <sup>m</sup> from Ref. [40]; <sup>n</sup> from Ref. [43]; <sup>o</sup> the sign of the entry was changed, see text for more details <sup>p</sup> the entry has no sign, negative sign is assumed, see text for more details; <sup>q</sup>  $\gamma = 60^\circ - \gamma$  is also possible; <sup>r</sup> pure E2 is assumed; <sup>s</sup> the transition has E0 component.

is overall agreement between the axial asymmetries derived by these three different methods, most often within one or two  $\sigma$  intervals. The discrepancies for the two Nd isotopes probably arise because of the presence of  $K = 0$  excited bands lying at very similar excitation energy to the  $2_1^+$  bands (resulting in mixing of the  $2_1^+$  states), while the Pt isotopes were already discussed above. Thus, the agreement observed in Fig. 3 validates the proposed determination of  $\gamma$  based on the  $R_{22\gamma/22}$  ratio. It should be noted that this method allows to determine  $\gamma$  with good precision even for near axially-symmetric nuclei; for instance, <sup>172</sup>Yb with  $\gamma_{R22\gamma/22} = 4.8(1)^\circ$ . The  $\gamma_{R22\gamma/22}$  deformations determined using the  $R_{22\gamma/22}$  ratios are illustrated in the right panel of Fig. 2 and listed in Tab. 1 for 27 nuclei, in addition to those previously determined through the  $\gamma_{TR}$  analysis [49, 50]. The values of  $\gamma$  derived from the  $R_{22/02}$  and  $R_{22\gamma/22}$  ratios are similar (except for <sup>198</sup>Hg), and describe shapes with all possible triaxialities.

It is important to stress that  $R_{22\gamma/22}$  analysis assigned triaxial shapes to all the 53 even-even rotating nuclei where  $\langle 2_1^+ \parallel \hat{E}2 \parallel 2_1^+ \rangle$  and  $\langle 2_1^+ \parallel \hat{E}2 \parallel 2_2^+ \rangle$  are known. This observation is in line with the suggestion that assumption-free analyses (such as the model-independent  $\gamma_{KC}$  evaluation based on multi-step Coulomb-excitation measurements with sufficient

statistics [45, 39, 46, 38, 35], and the generalized TR model), establish triaxial deformations for the vast majority of the studied nuclei. These findings suggest that ideal axially-symmetric prolate or oblate nuclear rotors may not be common.

In summary, this work proposes the use of simple ratios,  $R_{22/02}$  and  $R_{22\gamma/22}$ , of typically easy-to-measure E2 matrix elements ( $\langle 0_1^+ \parallel \hat{E}2 \parallel 2_1^+ \rangle$ ,  $\langle 2_1^+ \parallel \hat{E}2 \parallel 2_1^+ \rangle$  and  $\langle 2_1^+ \parallel \hat{E}2 \parallel 2_2^+ \rangle$ ) to extract the  $\gamma$  deformation of even-even rotating nuclei in a model-independent way. The approach is based on the Davidov-Filippov equations for the  $2_1^+$  and  $2_2^+$  states of even-even rotating nuclei. It is parameter-free because all assumptions of the model were either proven empirically (irrotational-flow dependence of the MoI from  $\gamma$ ) or become irrelevant (the spin dependence of the MoI). It requires experimental data on two matrix elements only, facilitating its application on a larger number of even-even rotating nuclei. The  $\gamma$  values determined using these ratios are in agreement with those established with the model-independent KC sum rules approach and the generalized TR model. The  $R_{22/02}$  ratio analysis allows the precise identification of triaxial deformations in the range  $20^\circ \lesssim \gamma_{R22/02} \lesssim 40^\circ$  using the E2 matrix elements of the  $2_1^+$  state alone; hence, opening the interesting prospect of determining

the triaxiality of exotic nuclei. As this approach does not require knowledge of the  $2^+_{\gamma}$  band, it is also very valuable for measuring triaxiality in nuclei where shape coexistence appears at low excitation energies and affects the corresponding  $\gamma$  band. The  $R_{22\gamma/22}$  ratio analysis needs knowledge of the  $\langle 2^+_{\gamma} || \hat{E}2 || 2^+_{\gamma} \rangle$  matrix element and is very sensitive in the full  $0^\circ < \gamma_{R22\gamma/22} < 60^\circ$  range. We report results from the proposed analyses on more than 60 even-even rotating nuclei where the axial asymmetries of the nuclear shapes are deduced in an assumption-free approach.

The work is based on research supported in part by the National Research Foundation of South Africa (Grant Number 150650).

## References

- [1] A. V. Afanasjev, H. Abusara, P. Ring, Nuclear fission in covariant density functional theory, in: EPJ Web Conf., Vol. 62, EDP Sciences, 2013, p. 03003.
- [2] E. Grosse, A. R. Junghans, R. Massarczyk, Broken axial symmetry as essential feature to predict radiative capture in heavy nuclei, Phys. Lett. B 739 (2014) 425–432.
- [3] M. A. Riley, A. Aguilar, A. O. Evans, D. J. Hartley, K. Lagergren, J. Ollier, E. S. Paul, A. Pipidis, J. Simpson, C. Teal, et al., Strongly deformed nuclear shapes at ultra-high spin and shape coexistence in N~90 nuclei, Acta Phys. Pol. B 40 (3) (2009) 513–522.
- [4] P. E. Garrett, T. R. Rodríguez, A. D. Varela, K. L. Green, J. Bangay, A. Finlay, R. A. E. Austin, G. C. Ball, D. S. Bandyopadhyay, V. Bildstein, et al., Multiple shape coexistence in  $^{110,112}\text{Cd}$ , Phys. Rev. Lett. 123 (14) (2019) 142502.
- [5] A. N. Bohr, B. R. Mottelson, Nuclear Structure (in 2 volumes), World Scientific Publishing Company, 1998.
- [6] D. J. Rowe, J. L. Wood, Fundamentals of nuclear models: foundational models, World Scientific Publishing Company, 2010.
- [7] P. Möller, R. Bengtsson, B. G. Carlsson, P. Olivius, T. Ichikawa, Global calculations of ground-state axial shape asymmetry of nuclei, Physical review letters 97 (16) (2006) 162502.
- [8] P. Möller, R. Bengtsson, B. G. Carlsson, P. Olivius, T. Ichikawa, H. Sagawa, A. Iwamoto, Axial and reflection asymmetry of the nuclear ground state, At. Data Nucl. Data Tables 94 (5) (2008) 758–780.
- [9] A. N. Bohr, The coupling of nuclear surface oscillations to the motion of individual nucleons, Mat. Fys. Dan. Vid. Selsk. 26 no. 14.
- [10] L. Wilets, M. Jean, Surface oscillations in even-even nuclei, Phys. Rev. 102 (3) (1956) 788.
- [11] A. S. Davydov, G. F. Filippov, Rotational states in even atomic nuclei, Nucl. Phys. 8 (1958) 237–249.
- [12] A. S. Davydov, V. S. Rostovsky, Relative transition probabilities between rotational levels of non-axial nuclei, Nucl. Phys. 12 (1) (1959) 58–68.
- [13] K. T. Hecht, G. R. Satchler, Asymmetric rotator model of odd-mass nuclei, Nucl. Phys. 32 (1962) 286–318.
- [14] V. Rezwani, G. Gneuss, H. Arenhövel, Dynamic collective model of the giant resonance, Phys. Rev. Lett. 25 (24) (1970) 1667.
- [15] V. Rezwani, G. Gneuss, H. Arenhövel, Further development of the dynamic collective model of the giant resonance, Nucl. Phys. A 180 (1) (1972) 254–272.
- [16] E. Bortolani, G. Maino, Isospin and deformation splittings of the giant dipole resonance for triaxial nuclei, Phys. Rev. C 43 (1) (1991) 353.
- [17] A. A. B. Mennana, M. Oulne, Giant dipole resonance in Sm isotopes within TDHF method, Eur. Phys. J. Plus 136 (1) (2021) 85.
- [18] R. Bengtsson, H. Frisk, F. R. May, J. A. Pinston, Signature inversion—a fingerprint of triaxiality, Nucl. Phys. A 415 (2) (1984) 189–214.
- [19] B. Ding, C. Petrache, S. Guo, E. Lawrie, I. Wakudyanaye, Z. Zhang, H. Wang, H. Meng, D. Mengoni, Y. Qiang, et al., Signature splitting of the g  $7/2$  [404]  $7/2+$  bands in  $^{131}\text{Ba}$  and  $^{133}\text{Ce}$ , Phys. Rev. C 104 (6) (2021) 064304.
- [20] O. Zeidan, D. J. Hartley, L. L. Riedinger, M. Danchev, W. Reviol, W. Weintraub, J.-y. Zhang, A. Galindo-Uribarri, C. J. Gross, S. D. Paul, et al., Rotational structures in  $^{129}\text{Nd}$  and signature splitting systematics of the  $\nu$  h11/2 bands in A~130 nuclei, Phys. Rev. C 65 (2) (2002) 024303.
- [21] F. Seiffert, W. Lieberz, A. Dewald, S. Freund, A. Gelberg, A. Granderath, D. Lieberz, R. Wirovski, P. Von Brentano, Band structures in  $^{126}\text{Xe}$ , Nucl. Phys. A 554 (2) (1993) 287–321.
- [22] S. Frauendorf, J. Meng, Tilted rotation of triaxial nuclei, Nucl. Phys. A 617 (2) (1997) 131–147.
- [23] E. A. Lawrie, O. Shirinda, Reaching degeneracy in two-quasiparticle chiral bands, Phys. Lett. B 689 (2-3) (2010) 66–71.
- [24] O. Shirinda, E. A. Lawrie, Multiple many-particle chiral systems described within the particle-rotor model, Eur. J. Phys. A 52 (2016) 1–7.
- [25] S. Frauendorf, F. Döna, Transverse wobbling: A collective mode in odd-A triaxial nuclei, Phys. Rev. C 89 (2014) 014322.
- [26] E. A. Lawrie, O. Shirinda, C. M. Petrache, Tilted precession and wobbling in triaxial nuclei, Phys. Rev. C 101 (3) (2020) 034306.
- [27] F. Xu, W. Satuła, R. Wyss, Quadrupole pairing interaction and signature inversion, Nucl. Phys. A 669 (1-2) (2000) 119–134.
- [28] B. Carlsson, I. Ragnarsson, Many-particles–plus–rotor description of magnetic bands at high spin, Phys. Rev. C 74 (4) (2006) 044310.
- [29] J. N. Orce, A. M. Bruce, A. Emmanouilidis, A. P. Byrne, G. D. Dracoulis, T. Kibédi, M. Caamaño, H. El-Masri, C. J. Pearson, Z. Podolyák, et al., Shape-driving effects in the triaxial nucleus,  $^{128}\text{Xe}$ , Phys. Rev. C 74 (3) (2006) 034318.
- [30] N. Marchini, A. Nannini, M. Rocchini, T. R. Rodríguez, M. Otanelli, N. Gelli, A. Perego, G. Benzoni, N. Blasi, G. Bocchi, et al., Emergence of triaxiality in  $^{74}\text{Se}$  from electric monopole transition strengths, Phys. Lett. B 844 (2023) 138067.
- [31] K. Kumar, Intrinsic quadrupole moments and shapes of nuclear ground states and excited states, Phys. Rev. Lett. 28 (4) (1972) 249.
- [32] D. Cline, Heavy ion coulomb excitation and nuclear structure, Annu. Rev. Nucl. Part. Sci. 36 (1986) 681–714.
- [33] B. Pritychenko, M. W. Herman, National nuclear data center: a worldwide user facility, Nucl. Phys. News 22 (3) (2012) 23–26.
- [34] Y. Toh, T. Czosnyka, M. Oshima, T. Hayakawa, H. Kusakari, M. Sugawara, Y. Hatsukawa, J. Katakura, N. Shinohara, M. Matsuda, Coulomb excitation of  $^{74}\text{Ge}$  beam, Eur. J. Phys. A 9 (2000) 353–356.
- [35] A. D. Ayangeakaa, R. V. F. Janssens, S. Zhu, D. Little, J. Henderson, C. Y. Wu, D. J. Hartley, M. Albers, K. Auranen, B. Bucher, et al., Evidence for rigid triaxial deformation in  $^{76}\text{Ge}$  from a model-independent analysis, Phys. Rev. Lett. 123 (10) (2019) 102501.
- [36] E. Clément, A. Görgen, W. Korten, E. Bouchez, A. Chatillon, J. P. Delaroche, M. Girod, H. Goutte, A. Hürstel, Y. Le Coz, et al., Shape coexistence in neutron-deficient krypton isotopes, Phys. Rev. C 75 (5) (2007) 054313.



- [37] E. Clément, M. Zielińska, A. Gørgen, W. Korten, S. Péru, J. Libert, H. Goutte, S. Hilaire, B. Bastin, C. Bauer, et al., Spectroscopic quadrupole moments in  $^{96,98}\text{Sr}$ : Evidence for shape coexistence in neutron-rich strontium isotopes at  $N=60$ , *Phys. Rev. Lett.* 116 (2) (2016) 022701.
- [38] J. Srebrny, T. Czosnyka, C. Droste, S. G. Rohoziński, L. Próchniak, K. Zajac, K. Pomorski, D. Cline, C. Y. Wu, A. Bäcklin, et al., Experimental and theoretical investigations of quadrupole collective degrees of freedom in  $^{104}\text{Ru}$ , *Nucl. Phys. A* 766 (2006) 25–51.
- [39] L. Svensson, C. Fahlander, L. Hasselgren, A. Bäcklin, L. Westerbergh, D. Cline, T. Czosnyka, C. Y. Wu, R. M. Diamond, H. Kluge, Multiphonon vibrational states in  $^{106,108}\text{Pd}$ , *Nucl. Phys. A* 584 (3) (1995) 547–572.
- [40] L. E. Svensson, Coulomb excitation of rotational nuclei, Ph.D. thesis, PhD thesis, Uppsala University (1989).
- [41] R. W. Ibbotson, C. A. White, T. Czosnyka, P. A. Butler, N. Clarkson, D. Cline, R. A. Cunningham, M. Devlin, K. G. Helmer, T. H. Hoare, et al., Quadrupole and octupole collectivity in  $^{148}\text{Nd}$ , *Nucl. Phys. A* 619 (1-2) (1997) 213–240.
- [42] C. Fahlander, I. Thorslund, B. Varnestig, A. Bäcklin, L. E. Svensson, D. Disdier, L. Kraus, I. Linck, N. Schulz, J. Pedersen, et al., Triaxiality in  $^{166}\text{er}$ , *Nucl. Phys. A* 537 (1-2) (1992) 183–206.
- [43] B. Kotliński, D. Cline, A. Bäcklin, K. G. Helmer, A. E. Kavka, W. J. Kernan, E. G. Vogt, C. Y. Wu, R. M. Diamond, A. O. Macchiavelli, et al., Coulomb excitation of  $^{168}\text{er}$ , *Nucl. Phys. A* 517 (2) (1990) 365–385.
- [44] C. Fahlander, B. Varnestig, A. Bäcklin, L. E. Svensson, D. Disdier, L. Kraus, I. Linck, N. Schulz, J. Pedersen, Coulomb excitation of  $^{172}\text{Yb}$ , *Nucl. Phys. A* 541 (1) (1992) 157–172.
- [45] C. Y. Wu, D. Cline, E. G. Vogt, W. J. Kernan, T. Czosnyka, K. G. Helmer, R. W. Ibbotson, A. E. Kavka, B. Kotlinski, R. M. Diamond, Electromagnetic properties of tungsten nuclei, *Nucl. Phys. A* 533 (2) (1991) 359–380.
- [46] C. Y. Wu, D. Cline, T. Czosnyka, A. Backlin, C. Baktash, R. M. Diamond, G. D. Dracoulis, L. Hasselgren, H. Kluge, B. Kotlinski, et al., Quadrupole collectivity and shapes of os and pt nuclei, *Nucl. Phys. A* 607 (2) (1996) 178–234.
- [47] K. Alder, A. Winther, On the theory of multiple coulomb excitation with heavy ions, *Mat. Fys. Dan. Vid. Selsk.* (1960) 253.
- [48] J. L. Wood, A. M. Oros-Peusquens, R. Zaballa, J. M. Allmond, W. D. Kulp, Triaxial rotor model for nuclei with independent inertia and electric quadrupole tensors, *Phys. Rev. C* 70 (2) (2004) 024308.
- [49] J. M. Allmond, J. L. Wood, Empirical moments of inertia of axially asymmetric nuclei, *Phys. Lett. B* 767 (2017) 226–231.
- [50] J. M. Allmond, presented at the CWAN-23 conference in China (2022).
- [51] P. Ring, P. Schuck, *The nuclear many-body problem*, Springer Science & Business Media, 2004.
- [52] D. J. Rowe, *Nuclear collective motion: models and theory*, Methuen and Co. Ltd., 1970.
- [53] H. Toki, A. Faessler, Asymmetric rotor model for decoupled bands in transitional odd-mass nuclei, *Nuclear Physics A* 253 (1) (1975) 231–252.
- [54] J. L. Wood, E. F. Zganjar, C. De Coster, K. Heyde, Electric monopole transitions from low energy excitations in nuclei, *Nucl. Phys. A* 651 (4) (1999) 323–368.
- [55] K. Heyde, J. L. Wood, Shape coexistence in atomic nuclei, *Rev. Mod. Phys.* 83 (4) (2011) 1467.
- [56] N. J. Stone, Table of nuclear electric quadrupole moments, *At. Data Nucl. Data Tables* 111 (2016) 1–28.
- [57] B. Pritychenko, M. Birch, B. Singh, M. Horoi, Tables of  $e2$  transition probabilities from the first  $2+$  states in even–even nuclei, *At. Data Nucl. Data Tables* 107 (2016) 1–139.
- [58] J. M. Allmond, J. L. Wood, W. D. Kulp, Triaxial rotor model description of quadrupole interference in collective nuclei: The  $p3$  term, *Phys. Rev. C* 80 (2) (2009) 021303.
- [59] K. Kumar, The signs of  $E2$ ,  $M1$  transition matrix elements of the tungsten, osmium and platinum nuclei, *Phys. Lett. B* 29 (1) (1969) 25–28.
- [60] D. Rhodes, B. A. Brown, A. Gade, S. Biswas, A. Chester, P. Farris, J. Henderson, A. Hill, J. Li, F. Nowacki, et al., Evolution of shape and collectivity along the Ge isotopic chain: The case of  $^{80}\text{Ge}$ , *Phys. Rev. C* 105 (2) (2022) 024325.
- [61] F. Becker, A. Petrovici, J. Iwanicki, N. Amzal, W. Korten, K. Hauschild, A. Hurstel, C. Theisen, P. A. Butler, R. A. Cunningham, et al., Coulomb excitation of  $^{78}\text{Kr}$ , *Nucl. Phys. A* 770 (3-4) (2006) 107–125.
- [62] J. Park, A. B. Garnsworthy, R. Kruecken, C. Andreoiu, G. C. Ball, P. C. Bender, A. Chester, A. Close, P. Finlay, P. E. Garrett, et al., Shape coexistence and evolution in  $^{98}\text{Sr}$ , *Phys. Rev. C* 93 (1) (2016) 014315.
- [63] W. D. Kulp, J. L. Wood, P. E. Garrett, C. Y. Wu, D. Cline, J. M. Allmond, D. Bandyopadhyay, D. Dashdorj, S. N. Choudry, A. B. Hayes, et al., Shape coexistence and mixing in  $^{152}\text{Sm}$ , [arXiv:0706.4129](https://arxiv.org/abs/0706.4129).
- [64] C. S. Lim, R. H. Spear, M. P. Fewell, G. J. Gyapong, Measurements of static electric quadrupole moments of the  $2+1$ ,  $2+2$ ,  $4+1$  and  $6+1$  states of  $^{196}\text{Pt}$ , *Nucl. Phys. A* 548 (2) (1992) 308–330.
- [65] J. Saiz-Lomas, M. Petri, I. Y. Lee, I. Syndikus, S. Heil, J. M. Allmond, L. P. Gaffney, J. Pakarinen, H. Badran, T. Calverley, et al., The spectroscopic quadrupole moment of the first  $2+$  state of  $^{12}\text{C}$ : A benchmark of theoretical models, *Phys. Lett. B* 845 (2023) 138114.
- [66] J. Henderson, G. Hackman, P. Ruotsalainen, S. Stroberg, K. Launey, J. Holt, F. Ali, N. Bernier, M. Bentley, M. Bowry, et al., Testing microscopically derived descriptions of nuclear collectivity: Coulomb excitation of  $^{22}\text{Mg}$ , *Phys. Lett. B* 782 (2018) 468–473.
- [67] R. H. Spear, Static quadrupole moments of first  $2+$  states in the  $2s$   $1d$  shell: A review of experiment and theory, *Phys. Rep.* 73 (5) (1981) 369–390.
- [68] L. P. Gaffney, J. Van de Walle, B. Bastin, V. Bildstein, A. Blazhev, N. Bree, J. Cederkäll, I. Darby, H. De Witte, D. DiJulio, et al., Low-energy coulomb excitation of  $^{62}\text{Fe}$  and  $^{62}\text{Mn}$  following in-beam decay of  $^{62}\text{Mn}$ , *Eur. J. Phys. A* 51 (2015) 1–9.
- [69] D. T. Doherty, J. M. Allmond, R. V. F. Janssens, W. Korten, S. Zhu, M. Zielińska, D. C. Radford, A. D. Ayangeakaa, B. Bucher, J. C. Batchelder, et al., Triaxiality near the  $^{110}\text{Ru}$  ground state from coulomb excitation, *Phys. Lett. B* 766 (2017) 334–338.